

Exploring inhibition of Pdx1, a component of the PLP synthase complex of the human malaria parasite *Plasmodium falciparum*

Shaun B. Reeksting*†, Ingrid B. Müller†, Pieter B. Burger*, Emmanuel S. Burgos‡, Laurent Salmon§, Abraham I. Louw*, Lyn-Marie Birkholtz* and Carsten Wrenger †||¹

* Department of Biochemistry, Faculty of Natural and Agricultural Sciences, University of Pretoria, Private Bag x20, Hatfield 0028, South Africa

† Bernhard Nocht Institute for Tropical Medicine, Department of Biochemistry, Bernhard Nocht-Straße 74, D-20359, Germany

‡ Albert Einstein College of Medicine, Biochemistry Department, 1300 Morris Park Avenue, Bronx, NY 10461, U.S.A.

§ Laboratoire de Chimie Bioorganique et Bioinorganique, CNRS-UMR 8182, Institut de Chimie Moléculaire et des Matériaux d'Orsay, Bâtiment 420, Univ Paris Sud XI, F-91405 Orsay, France

|| Department of Parasitology, Institute of Biomedical Science, University of São Paulo, Av. Prof. Lineu Prestes 1374, 05508-000 São Paulo-SP, Brazil

¹To whom correspondance should be addressed (Phone: +5511 3091 7335, Email: cwrenger@icb.usp.br).

Short title: Inhibition of *P. falciparum* PLP synthase

Keywords: Pyridoxal 5-phosphate (PLP), vitamin B₆, PLP synthase, Pdx1, inhibition, erythrose 4-phosphate (E4P).

Abbreviations: 4PEHz, 4-phospho-D-erythronhydrazide; ANCOVA, analysis of covariance; DHAP, dihydroxyacetone phosphate; DR5P, 2-deoxy-D-ribose 5 phosphate; DXP, 1-deoxy-D-xylulose 5-phosphate; E4P, D-erythrose 4-phosphate; EH_z, D-erythronhydrazide; G3P, DL-glyceraldehyde 3-phosphate; PLP, pyridoxal 5'-phosphate; PNP, pyridoxine 5'-phosphate; R5P, D-ribose 5-phosphate; Ru5P, D-ribulose 5-phosphate; RPI, R5P isomerase; RMS, root mean square; RMSD, root mean square deviation; TIM, triose phosphate isomerase.

Synopsis

Malaria tropica is a devastating infectious disease caused by *Plasmodium falciparum*. This parasite synthesizes vitamin B₆ *de novo* via the pyridoxal 5-phosphate (PLP) synthase enzymatic complex consisting of *PfPdx1* and *PfPdx2* proteins. Biosynthesis of PLP is largely performed by *PfPdx1*, ammonia provided by *PfPdx2* subunits, is condensed together with D-ribose 5-phosphate (R5P) and DL-glyceraldehyde 3-phosphate (G3P). *PfPdx1* accommodates both the R5P and G3P substrates and intricately coordinates the reaction mechanism, which is composed of a series of imine bond formations, leading to the production of PLP. We demonstrate that D-erythrose 4-phosphate (E4P) inhibits *PfPdx1* in a dose dependent manner. We propose that the acyclic phospho-sugar E4P, with a C1 aldehyde group similar to acyclic R5P, could interfere with R5P imine bond formations in the *PfPdx1* reaction mechanism. Molecular docking and subsequent screening identified the E4P hydrazide analogue, 4-phospho-D-erythronhydrazide (4PEHz), which selectively inhibited *PfPdx1* with an IC₅₀ of 43 μM. *PfPdx1* contained in the heteromeric PLP synthase complex was shown to be more sensitive to 4PEHz and was inhibited with an IC₅₀ of 16 μM. Moreover, the compound had an IC₅₀ value of 10 μM against cultured *P. falciparum* intraerythrocytic parasites. To further analyse the selectivity of 4PEHz, transgenic cell lines over-expressing *PfPdx1* and *PfPdx2* showed that additional copies of the protein complex conferred protection against 4PEHz, implicating that the PLP synthase is directly affected by 4PEHz *in vivo*. These *PfPdx1* inhibitors represent novel lead scaffolds which are capable of targeting PLP biosynthesis, and we propose this as a viable strategy for the development of newer therapeutics against malaria.

Introduction

The parasitic disease, malaria, caused by members of the genus *Plasmodium*, represents one of the most serious threats to humans worldwide. More than 2 billion people are exposed to the parasites leading to an estimated 500 million clinical cases and more than 1 million deaths per annum, mostly young children in Africa. An effective vaccine is not available and prophylaxis as well as chemotherapy depends solely on the administration of a small number of drugs [1, 2]. There are less than 30 different small molecule scaffolds or chemotypes that are effective against *P. falciparum* parasites, and the clinically-employed repertoire of antimalarials consists of only around 10 different scaffolds [3]. At the current rate of parasite drug-resistance development this handful of antimalarials are under threat of rapidly becoming ineffective. For this reason the discovery of newer chemical scaffolds and the exploitation of novel drug targets in this parasite are of utmost importance.

PLP is the catalytic active form of vitamin B₆ and a vital prosthetic group to a wide range of enzymes primarily involving amino acid biosynthesis [4]. The cofactor is extremely versatile, and partakes in enzyme-catalysed racemizations, transaminations, decarboxylations and substitution reactions [4]. During catalysis PLP functions to stabilize the negative charge at the C_α of a PLP-amino acid intermediate [4]. Recently, it became apparent that the function of PLP in *P. falciparum* parasites is not only restricted to its action as a prosthetic group. The molecule is required in response towards oxidative stress caused by the generation of singlet oxygen during hemoglobin digestion [5, 6]. Currently two known PLP-biosynthetic pathways exist; the 1-deoxy-D-xylulose 5-phosphate (DXP)-dependent pathway and the DXP-independent route. The DXP-dependent pathway is present in *Escherichia coli* and some proteobacteria [7]. The pathway involves several enzymes which condense D-erythrose 4-phosphate (E4P), DXP and glutamate to form pyridoxine 5'-phosphate (PNP), which is subsequently converted to PLP [8]. The DXP-independent pathway, consisting of the enzymes Pdx1 and Pdx2, is found in plants, fungi as well as the human pathogens

Plasmodium falciparum, *Toxoplasma gondii* and *Mycobacterium tuberculosis* [5, 9]. The pathway is independent of DXP and instead R5P, G3P and L-glutamine are utilised to form PLP. *P. falciparum* parasites have a functional DXP-independent pathway consisting of a PLP synthase, which is made up of *PfPdx1* and *PfPdx2*. Human hosts of the malaria parasite lack the biosynthetic enzymes and are unable to produce PLP, making this parasite-exclusive pathway an attractive target for the development of therapeutics.

The catalytic centre of the PLP synthase is Pdx1, where R5P, G3P and ammonia is combined through an intricately complex biochemical process [10]. Pdx1 proteins have been shown to alternatively utilise D-ribulose 5-phosphate (Ru5P) and dihydroxyacetone phosphate (DHAP) as substitute pentose and triose substrates, respectively [11-13]. The protein is therefore thought to contain R5P isomerase (RPI) and triose phosphate isomerase (TIM) activities in order to convert these alternative substrates. The reaction mechanism of PLP formation in Pdx1 has been extensively elucidated. The reaction in Pdx1 is initiated by R5P ring opening and the formation of an imine adduct between R5P and an internal K83 residue [10]. Initial binding of R5P to the internal K residue occurs via the C1 aldehyde group [10, 14]. Binding of R5P is followed by isomerization into an Ru5P intermediate, which eventually leads to the formation of an internal chromophore with characteristic absorbance at 320 nm, termed I₃₂₀ [10, 14, 15]. The addition of G3P to Pdx1 with bound I₃₂₀ forms leads to the formation and release of PLP [10]. It is thought that the furanose form of R5P is bound by Pdx1, however the exact mechanism of R5P ring opening remains unclear [15].

Here, we report the identification of *PfPdx1* inhibitors capable of interfering with PLP production. Analogues of R5P and G3P, in which stereo chemical arrangement and hydrolyzable phosphate groups were retained, were found to inhibit *PfPdx1* more effectively than their non-phosphorylated counterparts. The C1 aldehyde reactivity found on some of these inhibitors was also an important feature. Our studies revealed inhibitors with appreciable inhibitory effect against *P. falciparum* parasites *in vitro* and we demonstrated target specificity against *PfPdx1 in vivo*.

Experimental

Materials

D-Erythronhydrazide (EHZ) was synthesized by iThemba pharmaceuticals (South Africa) and supplied as HPLC purified product, which was structurally confirmed by ¹H-NMR and mass spectrometry. All other chemical compounds including R5P, G3P, E4P and D-erythrose were purchased from Sigma Aldrich unless otherwise stated. Albumax II and gentamycin were obtained from Invitrogen. [³H]-hypoxanthine (specific activity 30 Ci/mmol; 0.03 mM) was purchased from American Radiolabeled Chemicals and Ultima Gold scintillation fluid was from Perkin-Elmer. Restriction enzymes and ligases were purchased from New England Biolabs, USA. Oligonucleotides were obtained from Sigma Aldrich. The cloning vector pASK-IBA3, Strep-Tactin-Sepharose, anhydrotetracycline (AHT) and desthiobiotin were obtained from the Institut für Bioanalytik (IBA), Germany.

In silico modelling and ligand screening

Molecular modelling was performed using the Discovery Studio suite (v3.0, Accelrys Software Inc.) unless specified otherwise. *PfPdx1* homology models were generated using *T. maritima* (*TmPdx1*, PDB accession: 2ISS) and *Thermus thermophilus* (*TtPdx1*, PDB accession: 2ZBT) Pdx1 as templates. At the time this study was initiated the crystal structure of *P. berghei* Pdx1 (*PbPdx1*, PDB accession: 4ADU) [16] was not available. Several

homology models were created, each incorporating a different ligand from the template structures, including Ru5P and 2-methyl-2,4-pentanediol, as well as surrounding water molecules. The quality of the structures was assessed using model-derived pseudo-energy terms as well as stereochemical pseudo-energy terms and Ramachandran plots were generated in PDBsum [17, 18]. Analysis with PROCHECK showed a slight decrease in the average G factors between the crystal structure (0.39-0.41) and the homology models (0,00); scores above -0.5 are considered acceptable [17, 18]. The homology models were subjected to 200 steps of steepest descent energy minimization using the CHARMM forcefield with a root mean square (RMS) gradient tolerance of 0.1, followed by 200 steps conjugate gradient minimization. R5P was selected from the optimized protein-substrate complex to define a binding cavity and assigned a sphere radius of 8 Å. The defined binding cavity was used to extract pharmacophore features from the different *PfPdx1* models, followed by clustering and high throughput virtual screening of 2 million compounds of the Zinc database drug-like subset [19]. The database was generated as a multi-conformer composite database using catDB with a maximum of 250 representative conformations (Accelrys Software Inc.). The drug-like database was screened against 5 pharmacophore models and 300 best-hit compounds were identified based on their pharmacophore fit-values. These compounds were subjected to molecular docking simulations using LigandFit employing iterative rigid body minimization in a dreiding energy forcefield with 1500 Monte Carlo trials [20, 21]. The ligand poses were ranked according to the docking score (DockScore). In addition ligand poses were evaluated using LigScore empirical scoring functions [22]. R5P was used as control in cross-docking to validate ligand docking and scoring. Graphical displays were generated with VMD [23].

Following the release of the *PbPdx1* structure in 2012 [16], additional docking was performed on the *PfPdx1* homolog. The *PbPdx1* structure was prepared by removing the covalent bond between K84 and R5P, followed by minimization as described above. Post-minimization, R5P was selected to assign a binding site and sphere radius, similar to the docking simulations described above. K84 was maintained in a protonated state during the docking simulations (predicted pK_a of 12.1). Ligands were docked and scored using LigandFit and LigScore, as described above.

Mutagenesis of PfPdx1

Deletion of the C-terminal region of *PfPdx1* was performed on *PfPdx1* previously cloned in the expression plasmid pASK-IBA3 (IBA, Germany) [5]. Multiple deletion mutagenesis PCR's were set-up, and contained 35 ng of expression plasmid with 30 pmol each of the sense primer (5'-GCCGCGCGGTCTCGAATGGAAAATCATAAAGATGATGC-3') and antisense primer (5'-GCCGCGCGGTCTCAGCG*CTAACATCTAAAAGTATTTTAGGG-3') (site of C-terminal truncated region indicated with asterisk) in a final volume of 50 μ L with PCR Supermix (Invitrogen) containing recombinant *Thermus aquaticus* DNA polymerase. The cycling parameters were 95 °C for 3 min, then 35 cycles of 95 °C for 30 s, 41 °C for 90 s, 60 °C for 2 min. Parent template was removed from the reactions by incubation with 20 U of *DpnI* (New England Biolabs) for 2 h at 37 °C. Following Invitrogen Pure link PCR purification 50 μ L eluted solutions were digested with 10 U of *BsaI* (New England Biolabs) for 3 h at 37 °C, purified, and ligated (16 μ L) into similarly digested pASK-IBA3 expression plasmids at a ratio of 3:1 insert to vector using T4-DNA ligase (New England Biolabs). Ligation reactions (20 μ L) were transformed directly into 200 μ L XL10 Gold competent cells (Stratagene) using heat shock transformation for 60 s at 42°C, cooling on ice, followed by the addition of 800 μ L Luria-Bertani (LB) medium. Cells were plated onto LB agar plates containing 50 μ g/mL ampicillin (LB-amp) and grown for 16 h at 37°C. Single colonies were selected and used to inoculate 2 mL LB-amp medium, and grown for 16 h at 37°C. Plasmids were extracted using the peqGold plasmid miniprep kit I (Peqlab). Recombinant plasmids (10

μL) were confirmed through *Xba*I (5U) and *Hind*III (5U) (New England Biolabs) restriction enzyme digestions and automated sequencing (Seqlab, Germany). The *PfPdx1* R164A mutation was created with sense primer 5'-GCTATTAAACATATAG**GCA**ACTGTAAATAATGAA-3' and antisense primer 5'-TTCATTATTTACAGT**TGCT**TATATGTTTAATAGC-3' (mutated residues indicated in bold and underlined) as described previously [24].

Expression and purification of PfPdx1 and PfPdx2

PfPdx1 and *PfPdx2* clones in pASK-IBA3 were transformed into *E. coli* BLR (DE3) [5]. Selected single colonies were used to inoculate LB medium containing 50 $\mu\text{g}/\text{mL}$ ampicillin (LB-amp) and grown overnight at 37 °C. Cultures were diluted 1:100 into LB-amp media and grown to an OD₆₀₀ of 0.5. Expression was induced using 200 ng/mL AHT (IBA) and grown for 4 h at 37 °C with agitation. Cells were collected by centrifugation at 2000 *g* for 10 min and the pellets were resuspended in 100 mM Tris-HCl and 150 mM NaCl at pH 8.0. Phenylmethylsulfonyl fluoride (0.1 mM) and lysozyme (5 mg/10 mL reconstituted pellet) was added, the pellets sonicated using pulsing at output 6, duty cycle 40 with 1 min resting intervals on ice (Branson Sonifier 250) and clarified by centrifugation at 50000 *g* for 50 min at 4 °C. Strep-Tag fusion proteins were purified according to manufacturer's recommendations (IBA).

Enzyme activity measurements

PfPdx1 assays were performed using the 100 mM Tris-Cl and 150 mM NaCl buffer (pH 8.0) as previously described [25]. The *PfPdx1* assay contained 0.5 mM R5P, 0.5 mM G3P and 20 mM NH₄Cl in a final assay volume of 250 μL with 200 μg (6 nM) of purified *PfPdx1*. Initially compounds were only screened against *PfPdx1* to discount molecules that could have interfered with *PfPdx1* and *PfPdx2* heterodimerization. In assays containing both *PfPdx1* and *PfPdx2* 20 mM L-glutamine was used instead of NH₄Cl. Reactions used for baseline normalization included purified *PfPdx1* protein, G3P and NH₄Cl, without R5P. Reactions were incubated at 37 °C for 2.5 h and the PLP-Tris Schiff-base was detected at 414 nm. Spectrophotometric measurements, including wavelength scans, were performed with a Uvikon 933B spectrophotometer (Bio-Tek Kontron) in 70 μL cuvettes (Plastibrand, Brand) or using a Nanodrop 1000 (ND).

Culturing of P. falciparum and IC₅₀ assays

P. falciparum (3D7) parasites were maintained in continuous culture according to Trager *et al.* [26], as modified by Das Gupta *et al.* [27]. The RPMI 1640 culture medium contained 25 mM HEPES, 10 mM glucose, 20 mM sodium bicarbonate, 25 mM hypoxanthine and 0.5% w/v AlbuMAX II (Invitrogen) at pH 7.4. The RPMI 1640 media as supplied by Applichem contains 0.001 g/L or 4.86 μM pyridoxine hydrochloride. Parasite cultures were maintained at 4% hematocrit using human O+ erythrocytes in flasks (Nunc) with shaking at 200 rpm at 37°C. Parasite cultures (50 mL) consisting of ring stage parasites (1 to 5% parasitemia) were synchronized using 5% D-sorbitol every 48 h [28]. [³H]-Hypoxanthine incorporation assays were performed as described elsewhere [27] on ring stage parasites (2% hematocrit and 1% parasitemia) exposed to serial dilutions of test compound in 96 well plates at 37 °C. After 24 h, 100 nCi [³H]-hypoxanthine was added and parasites cultures were incubated for an additional 24 h, followed by cell harvesting (Inotech) and collection on filter mats. Filter mats were washed four times using distilled water, dried at 60°C for 10 min and suspended in 4 mL Ultima Gold™ scintillation fluid (Perkin Elmer) and counted using a Trilux liquid scintillation counter (Wallace). The 50% inhibitory concentrations (IC₅₀) were calculated from sigmoid dose response curves generated using GraphPad Prism 5 (GraphPad Software Inc.).

Long-term growth assays

Asynchronous *P. falciparum* parasites, co-transfected with *PfPdx1* and *PfPdx2* pARL1a⁻ vectors with blasticidin S and WR99210 antibiotic resistance, together with a mock cell line, containing vector with only antibiotic resistance, were maintained in culture, as described previously [6]. Blasticidin S-hydrochloride (Sigma Aldrich) and WR99210 (Jacobus Pharmaceuticals) were maintained at final concentrations of 2.1 mM and 5 nM, respectively. Long-term growth assays were performed, as previously described [29], using 12 well plates (Nunc) at 4% hematocrit, with 1% starting parasitemia. Both *PfPdx1/PfPdx2*-overexpressing and mock parasites were maintained in culture for 7 days. Spent media was removed from suspended erythrocytes by gently tilting the plates, and replaced with fresh media containing both antibiotics. Fresh 4PEHz was added to both treated-*PfPdx1/PfPdx2* as well as treated-mock parasites every day at a final concentration of 1 μM. The growth rate was assessed by morphological monitoring and counting of Giemsa-stained thin smears using oil immersion light microscopy at 100x magnification, counting ≥ 1000 red blood cells from each slide. The cumulative parasitemia was calculated using the determined parasitemia by factoring in the dilution. From the log transformed data the slope of the regression line was used to calculate the growth rate constant (K), by using the following equation;

$$K = \ln(10^{\text{slope}})$$

Results were analysed using GraphPad Prism 5 (GraphPad Software Inc.), in which the null hypothesis of equal regression lines slopes was tested at a 99% confidence interval ($P = 0.01$). Analysis of covariance (ANCOVA) was conducted (JMP, Version 9, SAS Institute Inc.), testing whether the slopes significantly differed from each other with $\alpha = 0.05$.

Results

In silico docking and screening of *PfPdx1* inhibitors

Homology models of *PfPdx1* were generated from *T. maritima* (*TmPdx1*) and *T. thermophilus* (*TtPdx1*) Pdx1 templates that share a 60% and 61% sequence identity with *PfPdx1*, respectively. The resulting models showed an average RMSD of 3.7 Å and 2.4 Å compared to the C_α backbone of the *TmPdx1* and *TtPdx1* templates, respectively. Comparing the active site residues (residues within 5 Å of the substrates) revealed a high degree of structural conservation with RMSD values of 0.7 Å and 1.0 Å, respectively. Moreover, a structural comparison of our models to the recently released *P. berghei* Pdx1 (*PbPdx1*), which shares a 85% sequence identity with *PfPdx1*, showed a highly conserved C_α backbone RMSD ranging between 1.2 Å and 1.3 Å. Moreover, the active site residues of the *PfPdx1* models showed RMSD values of between 0.6 Å and 0.7 Å, confirming the quality and validity of the models. Five diverse pharmacophore models descriptive of the *PfPdx1* R5P binding site were derived from the protein models and screened against the drug-like subset of the Zinc database. Using the 300 best-fitting compounds, additional molecular docking was used to refine and determine binding capabilities in the R5P active site (Table 1). Following docking, a total of 19 compounds were selected for *in vitro* testing against purified *PfPdx1* whereby PLP formation was monitored at a wavelength of 414 nm according to Wrenger *et al.* [5], (Table 1). Compounds 1-4 contained sulfonate moieties and showed similar docking scores to that of R5P, however had no appreciable activity against *PfPdx1* at 3 mM (Table 1). Four polyhydroxylated compounds were identified from the *PfPdx1* pharmacophores (compounds 5-8). Compound 8 which had a terminal keto-ester arrangement was the most effective of the

polyhydroxylated compounds tested, with a 12% reduction of *PfPdx1* activity at 0.5 mM, although not statistically significant (Table 1). Compounds **9**, **13** and **16**, which share a pyrimidine sulfonamide moiety, were not effective at inhibiting *PfPdx1* (Table 1). Fosmidomycin (compound **17**), which was predicted to have a high docking score, had no inhibitory effect on *PfPdx1* activity at 20 mM (Table 1).

We investigated whether molecules closely related to the *PfPdx1* substrate R5P were capable of inhibiting the protein. The R5P analogues, 2-deoxy-D-ribose 5 phosphate (DR5P, compound **18**) and 1-deoxy-D-xylulose 5-phosphate (DXP, compound **19**), had similar docking scores compared to R5P (Table 1). This suggested that DR5P could have favourable binding interactions in the R5P-binding site. When tested, DR5P was a weak inhibitor of *PfPdx1* even at concentrations as high as 12 mM with 56% ($P < 0.10$) of the enzyme activity remaining (Figure 1A). DXP decreased *PfPdx1* activity to 88% at 5 mM (Table 1). Considering that initial binding of R5P to Pdx1 entails imine formation with K83, DR5P could compete for this interaction [15]. Spectrophotometric UV-visible absorbance spectra of *PfPdx1* incubated with DR5P revealed minor decreases in I_{320} formation with increasing concentrations of DR5P (Figure 1A). Decreased PLP production suggested that the molecule could potentially interfere with R5P-K83 imine adduct formation and/or PLP formation.

The specificity and stringency of *PfPdx1* for other R5P analogues that could be either incorporated into the PLP ring structure and/or interfere with R5P imine adduct formation, was tested next. Several sugars including E4P, F6P, DR5P (Figure 1B) and DXP (results not shown) did not support the formation of PLP, confirming the strict substrate specificity of *PfPdx1*. Interestingly we noted that substitution of R5P by E4P resulted in the formation of the single I_{320} chromophore similar to *PfPdx1* incubated with R5P in the absence of G3P (Figure 1B). The structural resemblance between E4P and R5P suggests that the former could compete with R5P for Schiff base formation with the internal K83 residue. Molecular docking simulations predicted similar LigScores for E4P and R5P in *PfPdx1* models (Table 2). Similarly, docking of E4P into the *PbPdx1* was comparable to the R5P substrate (Figure 1C, Table 2). E4P was orientated with the aldehyde group in close proximity to the K84 residue (Figure 1D). These predicted interactions were investigated in more detail below.

Intensive analysis of E4P as PfPdx1 inhibitor

The activity of *PfPdx1* was assayed in the presence of varying concentrations of E4P, and a dose-dependent decline in PLP synthesis was observed (Figure 2A). A concomitant increase in absorbance at 320 nm was observed for increasing concentrations of E4P (Figure 2A). To discard potential conjugation or adduct formation of PLP by E4P, calibration curves of increasing concentrations of PLP were used to show that 1 mM E4P did not significantly affect detection of PLP at 414 nm ($n = 4$, $P = 0.975$, Suppl. Figure 1). This confirmed that E4P was responsible for inhibiting the production of PLP by *PfPdx1*. E4P inhibited the formation of PLP by *PfPdx1* with an IC_{50} value of 3.7 ± 0.9 mM (Figure 2B, Table 2). The unphosphorylated analogue of E4P - D-erythrose - similarly interfered with PLP formation but was more than 40 times weaker compared to E4P (Figure 2B, Table 2). This emphasized the role of such hydrolyzable phosphate groups with the additional negative charge potentially facilitating entry into the *PfPdx1* active site.

Residues involved in I₃₂₀ formation

Recent studies have revealed several important residues involved in I_{320} formation and include D26, K83 and K151 [24] as well as residues from the C-terminus [30]. We sought to verify the importance of these residues during *PfPdx1* I_{320} formation. Incubation of R5P with both WT Pdx1 and ERR (E136A, R139A and R140A) *PfPdx1* resulted in I_{320} formation, however, the DKK (D26A, K83A and K151A) mutant was unable to form this species (Figure 3A).

This corroborates previous findings and excludes the involvement of the ERR residues located in the PLP binding site in I₃₂₀ formation [31]. A RHE (R85A, H88A and E91A) *PfPdx1* mutant was previously shown to prevent dodecameric assembly, and to be incapable of activating *PfPdx2* subunits [24]. These residues are therefore believed to coordinate Pdx1-Pdx1 subunit cross talk. Additional experimentation with RHE *PfPdx1* mutants and Δ C Pdx1, lacking the \pm 30 C-terminal residues, revealed that both proteins were unable to form I₃₂₀ (Figure 3B). These observations are in agreement with functions assigned to the C-terminal region and moreover emphasized the importance of the RHE residues for R5P binding and imine adduct formation [30]. Reduced formation of I₃₂₀ in R167A *PfPdx1* suggested that this residue, which is part of the G3P binding site, indirectly influences the way R5P is processed (Figure 3C). Contrary to observations elsewhere, this mutation decreased enzyme activity by only ~50% (Figure 3C) [13].

E4P analogues show inhibitory activity against PfPdx1

From the E4P lead structure a closely related hydrazide analogue 4PEHz [32], and the unphosphorylated form of 4PEHz, termed EHz, were selected and tested against *PfPdx1*. Previously, 4PEHz was shown to have weak inhibitory activity against spinach RPI [32]. Molecular docking simulations predicted favourable ligand poses for 4PEHz in the R5P cavity of *PfPdx1*, as well as in *PbPdx1* (Table 2). The EHz molecule was predicted to have less favourable binding interactions in *PfPdx1* and had smaller Ligscore binding affinities compared to 4PEHz (Table 2). 4PEHz could be docked into the *PbPdx1* and had hydrazide groups orientated in close proximity to K84, with hydrogen bonds predicted to form between the ketone substituent of 4PEHz and K84 (Figure 4A). Enzyme preparations of *PfPdx1* with 4PEHz revealed a concentration dependent decrease in PLP formation, with visible increases in a 320 nm chromophoric species (Figure 4B). Kinetic assays revealed 4PEHz as an effective inhibitor with an IC₅₀ of 43 ± 8 μ M, whereas EHz was more than 20 times weaker (Figure 4C, Table 2). Interestingly, when tested on the *PfPdx1* component of the glutamine-dependent PLP synthase complex, containing *PfPdx2*, 4PEHz had an IC₅₀ of 16 ± 4 μ M (Figure 4D).

Effect of 4PEHz and EHz on cellular level

The effect of 4PEHz and EHz was determined on *P. falciparum* parasite proliferation. After 48 h incubation of intra-erythrocytic *P. falciparum* parasite cultures with 4PEHz an IC₅₀ of 10.4 ± 1.2 μ M was determined (Figure 5A). The unphosphorylated EHz was 13-fold weaker compared to 4PEHz, with an IC₅₀ of 138 ± 9 μ M (Figure 5A). To further elucidate the mode of action of 4PEHz *in vivo* the compound was tested on *P. falciparum* over-expressing *PfPdx1/PfPdx2* parasites [6]. Both mock control and *PfPdx1/PfPdx2* over-expressing parasite proliferation was monitored over a seven-day period in the presence of 1 μ M 4PEHz. The proliferation of mock-parasites treated with 4PEHz significantly decreased over the course of 168 h (Figure 5B). Relative to control mock parasites the proliferation was significantly ($p < 0.05$) affected by 4PEHz only after 48 h, and the parasite growth diminished to 10% of control parasites after 168 h. In contrast, parasites overexpressing *PfPdx1* and *PfPdx2* were not significantly affected by 4PEHz treatment, and showed a relatively unchanged growth profile up until 144 h. After 168 h the growth of the *PfPdx1/PfPdx2* over-expressing parasite growth was not significantly different from untreated control parasites. This suggested that complementation of PLP biosynthesis through over-expression of *PfPdx1* and *PfPdx2* protects the parasites from the effects of 4PEHz.

Additionally, the growth rate constants (K) of mock and *PfPdx1/PfPdx2* over-expressing parasites were compared using logarithmic growth curves (Suppl. figure 2). The slopes of the fitted lines were used to calculate the growth rate constant which represents the increase in parasite growth per unit time. The growth rate constant (K) of the mock parasites treated with 4PEHz was smaller than that of untreated-mock parasites. Statistical analyses comparing the

slopes of the mock treated and mock-untreated fitted lines revealed a significant difference with accompanying analysis of covariance (ANCOVA) confirming this observation. This indicates that 4PEHz had an effect of parasite growth. In contrast, *PfPdx1* and *PfPdx2* over-expressing parasites had similar growth rate constants, and the slope of the fitted lines were not statistically different, indicating that the growth rate of the *PfPdx1/PfPdx2*-overexpressing parasites was unaffected by 4PEHz-treatment. The effect of 4PEHz on the parasite life-stage composition was also investigated (Suppl. figure 3 and 4). During the seven day treatment period with 4PEHz the ring and trophozoite parasites from mock treated parasites had significantly different growth compositions on a single day when compared to untreated mock parasites (Suppl. figure 3). In contrast, the *PfPdx1/PfPdx2* parasite life-stage compositions remained relative unchanged and no significant differences in parasite stage growth was observed (Suppl. figure 4). The complementation of PLP biosynthesis rescued the parasites from the effects of 4PEHz, and also suggests that 4PEHz affects *PfPdx1*-related processes within the parasites.

Discussion

With antimalarial drugs being rendered ineffective at alarming rates newer chemical leads aimed at targeting diverse metabolic pathways are required. The malaria parasite depends on *de novo* biosynthesis of PLP by PLP synthase and the cofactor plays an essential role during amino acid metabolism and folate biosynthesis [7]. PLP-dependent enzymes involved in amino acid biosynthesis principally bind PLP via an imine bond or Schiff base through utilizing an active site lysine residue [33]. PLP has recently been ascribed potent antioxidant roles and has been proposed to aid in reducing parasite oxidative stress associated with heme and free-iron release during digestion of host erythrocyte hemoglobin [6, 34]. The components of the PLP synthase are up-regulated when parasites are exposed to singlet molecular oxygen ($^1\text{O}_2$), and through protein complementation *PfPdx1* and *PfPdx2* were directly associated with detoxification of $^1\text{O}_2$ [6]. PLP biosynthesis is indispensable to the parasites and this pathway is also absent from humans making it an ideal target for the development of chemotherapeutics.

Three distinct sites for binding of the reaction substrates and products have been identified on Pdx1. Crystallographic evidence for the R5P binding site was provided from *Thermotoga maritima* Pdx1 (*TmPdx1*) with Ru5P bound via an imine to the K82 residue (equivalent to *PfPdx1* K83) [31]. In the *Saccharomyces cerevisiae* Pdx1 structure an additional site, previously observed to contain a phosphate ion, was shown to accommodate PLP [12, 13, 31]. Residues of the PLP binding site in *PfPdx1* include the highly conserved ERR triad comprising E136, R139 and R140, which interact mainly with the phosphate groups of PLP [13, 24]. Moreover, a site which contained G3P was identified and involved R164 (equivalent to R167 in *PfPdx1*) [13]. The R5P, PLP and G3P binding sites are located more than 10 Å from each other and, even though much is known regarding the reaction mechanism, some questions regarding substrate mobility and dynamics from these distant binding sites remains to be uncovered.

The Pdx1 protein of PLP synthase is highly conserved, and could imply evolutionary maintenance of specialized function [34, 35]. Mechanistic elucidation of the Pdx1 reaction coordinate has highlighted the multitude of complex mechanistic steps involved in forming PLP [10, 11, 15]. The reaction mechanism consists of several imine bond formations [10]. Initial binding of R5P entails formation of an imine with a Pdx1 lysine residue (Figure 6) followed by isomerization into a Ru5P imine adduct. The bound intermediate is subsequently converted into the I₃₂₀ chromophore, which forms an imine bond with G3P, and undergoes ring closure to ultimately form PLP (Figure 6) [10]. Both substrates R5P (acyclic-forms) and

G3P have reactive C1 aldehyde groups and are phosphorylated. The α -hydroxy or C1 aldehyde group on both R5P and G3P is essential for initial substrate binding, I₃₂₀ formation as well as G3P-binding. The G3P-phosphate group forms part of the final PLP molecule, whereas the R5P-phosphate group is eliminated during the reaction mechanism (Figure 6) [10]. In *TmPdx1* the R5P-phosphate group was shown to form H-bonds with three glycine amide nitrogen atoms and could function to facilitate orientation of the molecule during catalytic conversion [13].

We sought to identify molecules which could be accommodated within the R5P active site of *PfPdx1*, possibly affecting PLP formation, which would make attractive starting points for the development of novel antimalarials. Virtual screening of the *PfPdx1* R5P-binding site pharmacophores identified compounds with diverse chemical scaffolds. Several polyhydroxylated compounds with similar sugar-like backbone to R5P were identified, however were not effective at inhibiting *PfPdx1*. Compounds with terminal sulfonate groups, which were predicted to mimic phosphate groups of R5P in the R5P-binding cavity were ineffective at inhibiting *PfPdx1*. The reasons for this became clear when we tested closely-related analogues of R5P, which were more effective at inhibiting *PfPdx1*. Initial binding to *PfPdx1* requires Schiff-base adduct or imine formation with internal K-residues, and computationally-predicted compounds were not capable of this due to the lack of reactive functional groups.

DR5P inhibited *PfPdx1*, and marginally reduced formation of I₃₂₀ suggesting that DR5P may compete with R5P, albeit weakly. Following the currently proposed reaction mechanism of *PfPdx1*, DR5P would be accommodated by *PfPdx1* and potentially bind to the K83 residue [10]. The DR5P-adduct might not undergo conversion due to the lack of the C2 hydroxyl substituent, which could affect the resident time within the active site, possibly explaining the lack of potency of DR5P. E4P effectively inhibited *PfPdx1*. Structurally E4P is similar to R5P, with one less carbon and hydroxyl substituent. We speculated that E4P could be interfering with R5P binding in *PfPdx1*. Docking simulations predicted that E4P could occupy the R5P-binding site and that the sugar-derived hydroxyl substituents as well as phosphate moiety have favourable H-bonding interactions within this site. E4P could outcompete R5P for K83 imine formation, and potentially also undergo conversion similar to R5P (Figure 6). This would affect binding of R5P and lead to disrupted PLP formation. The E4P-analogue DXP, with a terminal ketone group, was not an effective inhibitor. This suggested the C1 aldehyde reactivity, as found on E4P, was important for inhibition and this feature could possibly determine entry into the R5P active site. D-erythrose was almost 50-times weaker than E4P suggesting that the phosphate group is also essential for efficacy. Similar to R5P, the phosphate group of E4P might facilitate orientation of the molecule in the R5P-binding site. The structure-activity relationship of E4P and analogues suggested that both the terminal α -hydroxy C1 aldehyde- and hydrolyzable phosphate-group arrangements were important for effective inhibition of *PfPdx1*.

Spinach RPI is inhibited by E4P, and more so by 4-phosphoerythronic acid [36]. The weak RPI activity of *PfPdx1* could therefore similarly be targeted by such molecules. Glucose-6-phosphate isomerases (GPI) are inhibited by acyclic phospho-sugars which have free carbonyl groups, like E4P [37-39]. Moreover, the GPI active site resembles that of triosephosphate isomerases (TIM) – a function that has been implicated in Pdx1 proteins [40, 41]. Even though no definitive site for DHAP isomerization has been found, the implicated TIM-function of *PfPdx1*, albeit weak, could be affected by E4P [13, 14]. Therefore an alternative mode of action of E4P could involve binding to the postulated G3P-binding site [13]. E4P might interact with K120 (equivalent to *ScPdx1* K117), whereby E4P would mimic G3P, potentially interfering with downstream PLP ring-closure steps. E4P could therefore either affect the RPI- or TIM-activities in *PfPdx1*.

Our studies suggest for the first time that the naturally occurring E4P metabolite could regulate PLP production in *P. falciparum* parasites through inhibition of *PfPdx1*. Considering that the DXP-dependent pathway in *E. coli* utilizes the E4P precursor for the production of PLP [42], it is interesting from an evolutionary point of view that this molecule inhibits the plasmidial Pdx1 in the DXP-independent pathway. E4P is a vital precursor for the production of chorismate, and downstream phenylalanine, tyrosine and *p*-aminobenzoic acid, utilized for the production of folates [43]. The pathway for the production of E4P from sedoheptulose 7-phosphate by transaldolases has not been identified in *P. falciparum* [44], however transketolases are known to produce E4P from F6P and G3P [45]. E4P is an indispensable metabolite to the parasites and future studies might aim to explore the *in vivo* effects of E4P fluctuations on PLP production.

From the *TmPdx1* structure it was shown that D26 and K83 constitute the R5P binding site, therefore could be directly involved in I₃₂₀ formation [31, 46]. Our observations for the DKK *PfPdx1* mutant confirmed previous results, and residues involved in I₃₂₀ formation are most probably D26 and K83 in *PfPdx1* [15, 31]. Moreover, our findings support previous results which showed that the Δ C-terminal Pdx1 mutant is incapable of forming I₃₂₀ [30]. Residues R139 and R140 of the ERR motif forms part of the PLP binding site [13, 31, 46]. Mutation of these residues was previously shown to abolish *PfPdx1* activity, underscoring their catalytic importance most likely during PLP binding and release [24]. Our observations revealed that the ERR *PfPdx1* variant was still able to form I₃₂₀. This suggested that these residues were not directly involved in R5P isomerization leading to formation of the chromophore. The highly conserved residues R85, H88 and E91 from the RHE motif of *PfPdx1*, located on the loop between β 3 and α 3, are essential for Pdx1 hexamer assembly and subsequent Pdx2 binding and activation [24]. These residues were suggested to facilitate Pdx1 hexameric pre-assembly, which is coordinated and a prerequisite for PLP synthase activation [24]. In the absence of *PfPdx2*, the RHE triple mutant was also incapable of forming the I₃₂₀ specie. Lack of I₃₂₀ formation in the RHE mutant indicates that these residues are intricately involved in R5P binding, additionally taking part in active site reorganisation during dodecamer assembly. A glycine residue (G84) located on the same loop region as these RHE residues was shown to form H-bonds with D110 and a water molecule which forms part of the G3P binding site [13]. This suggests that the RHE-containing loop region is vital for both assembly and enzyme activity and emphasizes that Pdx1:Pdx1 interactions, involving these RHE residues, could serve as a target site for the development of novel target-based inhibitors.

The moderate inhibitory efficacy of E4P against *PfPdx1* motivated testing of E4P analogues against the enzyme. 4PEHz inhibited *PfPdx1* and the entire PLP synthase complex with low micromolar efficacy. During oligomerization of Pdx1 and Pdx2 into the functional PLP synthase Pdx1 activates the glutaminase activity in Pdx2 monomers leading to the formation of a putative opening through which ammonia is channelled [12]. Oligomerization also leads to increased R5P binding affinity in Pdx1 [47]. We noted increased inhibitory efficacy of 4PEHz in the *PfPdx1*:*PfPdx2* complex suggesting improved binding interactions of 4PEHz, similar to previous observations for R5P, and thus that 4PEHz may bind in the R5P binding site. 4PEHz was previously reported as a weak inhibitor of spinach RPI with a K_i of 1.8 ± 0.2 mM [32]. 4PEHz structurally mimics the 1,2-*cis*-enediolate intermediate in the RPI isomerization step [32]. The lead us to speculate that 4PEHz could affect the RPI activity of *PfPdx1*. Both EHz and 4PEHz can potentially form Schiff-bases with PLP through linkage with hydrazide groups. However, the difference in inhibitory efficiency, indicated by involvement of the phosphate group, suggests that the enzyme preferentially allows entry of more negatively charged molecules like 4PEHz. Similar observations for E4P compared to D-erythrose also support this hypothesis. In both E4P and 4PEHz the presence of hydrolyzable phosphate groups improved inhibitory activity and suggests that these two molecules could similarly occupy the R5P binding site on the protein, which is also supported by *in silico*

docking results. As outlined in Figure 6, 4PEHz shares chemical similarities to both E4P and R5P, suggesting a similar mode of action compared to E4P.

4PEHz inhibited parasite growth at low micromolar concentrations, compared to the unphosphorylated EHz analogue, which was at least 12-fold weaker. PLP is an essential cofactor, and continuously recycled within the parasite, therefore expectedly attenuation of PLP biosynthesis has a dramatic effect on parasite proliferation. The complementation of *PfPdx1* and *PfPdx2* in *P. falciparum* parasites *in vivo* was shown to increase tolerance to cercosporin-induced oxidative stress [6, 48]. Here we similarly observed that parasites which over-express *PfPdx1* and *PfPdx2* were not affected by the *PfPdx1*-inhibitor 4PEHz. In contrast, parasites harbouring the same expression plasmid, without *PfPdx1* and *PfPdx2*, had reduced growth rates and were significantly attenuated by 4PEHz. Almost 3-fold greater PLP levels were previously reported in *PfPdx1/PfPdx2* complemented parasites [6]. This complementation of PLP synthesis *in vivo* counteracts the effects of 4PEHz, and suggests that 4PEHz interferes primarily with this part of the parasite metabolism. These results support 4PEHz as a novel lead compound for targeting vitamin B₆ biosynthesis within the malaria parasite.

Endogenous pyridoxal/pyridoxine salvage pathways might be capable of complementing the PLP pool in the parasites and could diminish the effects of *PfPdx1* inhibitors. Indeed the parasite possesses a functional pyridoxal kinase (PdxK), which activates salvaged B₆ vitamers. This pathway has successfully been exploited using prodrugs which are trapped in the parasite upon phosphorylation by PdxK [29]. Once phosphorylated these PLP analogues were shown to disrupt PLP-dependent processes and thus kill the parasite selectively [29]. However, pyridoxal is bound to hemoglobin and such not available for uptake. Furthermore the parasite shows no growth defect when cultured in pyridoxine free medium [7]. Since 4PEHz inhibits parasite proliferation in culture media containing approximately 5 μ M pyridoxine this suggests that 4PEHz is effective irrespective of endogenous B₆ salvage pathways. Nevertheless, in combination with this strategy, compounds that directly target *PfPdx1* may contribute even more effectively by additionally starving the parasites of PLP and thus leading to parasite death.

Novel lead scaffolds were identified against *PfPdx1*, and were capable of targeting PLP biosynthesis within the *P. falciparum* parasites. Lead compounds should ideally have greater potency, and undoubtedly these compounds will have to undergo further optimization to improve their efficacy. These relatively simplistic, low-molecular weight compounds are well suited for additional molecular weight contributions from chemical modifications or functionalization during scaffold modifications. These compounds had structural complementarity to R5P and more noticeably contained relatively reactive C1 groups. Compounds containing reactive functional groups are undesirable optimization starting points and would normally have been removed from high-throughput or virtual screening libraries [49, 50]. A successful antimalarial with a similar chemical structure is the isoprenoid precursor pathway inhibitor fosmidomycin, with terminal aminoaldehyde arrangement [51, 52]. The nature of *PfPdx1*, its substrates, and the reaction mechanism also needs to be considered in order to achieve better inhibitor efficacy. Additionally the mode and site of binding in *PfPdx1* will need to be determined, and may provide insights into the mode of action of these inhibitors.

Acknowledgments

S. R. conducted part of this work in fulfilment of the requirements for a Ph.D. from the University of Pretoria.

Author contributions

Devised experimental procedures and strategies: SR IM PB EB LS AL LB CW. Conducted experiments: SR IM CW. Manuscript preparation: IM PB EB LS AL LB CW.

Funding

This work was funded by the grants [WR 124/2] and [WR 124/3] from the Deutsche Forschungsgemeinschaft (DFG) to CW as well as the National Research Foundation (NRF) of South Africa [65876] and NRF-DFG Scientific exchange grants to LMB, IM and CW. SBR was supported by the PhD sandwich programme of the German Academic Exchange Programme (DAAD) [A/08/99008]. CW is supported by grant [2009/54325-2] from the Fundação de Amparo à Pesquisa do Estado de São Paulo (FAPESP) within the “Jovem Pesquisador” programme.

References

- 1 Greenwood, B. M., Fidock, D. A., Kyle, D. E., Kappe, S. H. I., Alonso, P. L., Collins, F. H. and Duffy, P. E. (2008) Malaria: progress, perils, and prospects for eradication. *J. Clin. Invest.* **118**, 1266-1276
- 2 Greenwood, B. M. (2008) Control to elimination: implications for malaria research. *Trends Parasitol.* **24**, 449-454
- 3 Guiguemde, W. A., Shelat, A. A., Garcia-Bustos, J. F., Diagana, T. T., Gamo, F. J. and Guy, R. K. (2012) Global Phenotypic Screening for Antimalarials. *Chem. Biol.* **19**, 116-129
- 4 Eliot, A. C. and Kirsch, J. F. (2004) Pyridoxal phosphate enzymes: mechanistic, structural, and evolutionary considerations. *Annu. Rev. Biochem.* **73**, 383-415
- 5 Wrenger, C., Eschbach, M., Müller, I. B., Warnecke, D. and Walter, R. D. (2005) Analysis of the vitamin B6 biosynthesis pathway in the human malaria parasite *Plasmodium falciparum*. *J. Biol. Chem.* **280**, 5242-5248
- 6 Knöckel, J., Müller, I. B., Butzloff, S., Bergmann, B., Walter, R. D. and Wrenger, C. (2012) The antioxidative effect of de novo generated vitamin B6 in *Plasmodium falciparum* validated by protein interference. *Biochem. J.* **443**, 397-405
- 7 Müller, I. B., Hyde, J. E. and Wrenger, C. (2010) Vitamin B metabolism in *Plasmodium falciparum* as a source of drug targets. *Trends Parasitol.* **26**, 35-43
- 8 Cane, D. E., Du, S., Robinson, J. K., Hsiung, Y. and Spenser, I. D. (1999) Biosynthesis of vitamin B6: enzymatic conversion of 1-deoxy-D-xylulose-5-phosphate to pyridoxol phosphate. *J. Am. Chem. Soc.* **121**, 7722-7723
- 9 Knöckel, J., Müller, I. B., Bergmann, B., Walter, R. D. and Wrenger, C. (2007) The apicomplexan parasite *Toxoplasma gondii* generates pyridoxal phosphate *de novo*. *Mol. Biochem. Parasitol.* **152**, 108-111
- 10 Hanes, J. W., Keresztes, I. and Begley, T. P. (2008) ¹³C NMR snapshots of the complex reaction coordinate of pyridoxal phosphate synthase. *Nat. Chem. Biol.* **4**, 425-430
- 11 Gengenbacher, M., Fitzpatrick, T. B., Raschle, T., Flicker, K., Sinning, I., Müller, S., Macheroux, P., Tews, I. and Kappes, B. (2006) Vitamin B6 biosynthesis by the malaria parasite *Plasmodium falciparum*. *J. Biol. Chem.* **281**, 3633-3641
- 12 Strohmeier, M., Raschle, T., Mazurkiewicz, J., Rippe, K., Sinning, I., Fitzpatrick, T. B. and Tews, I. (2006) Structure of a bacterial pyridoxal 5'-phosphate synthase complex. *Proc. Natl. Acad. Sci. USA.* **103**, 19284-19289

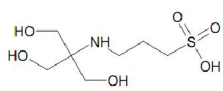
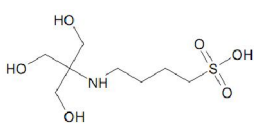
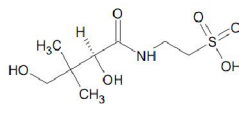
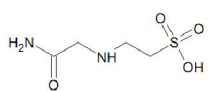
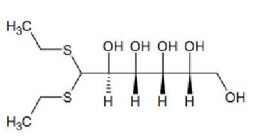
- 13 Zhang, X., Teng, Y., Liu, J., He, Y., Zhou, K., Chen, Y. and Zhou, C. (2010) Structural insights into the catalytic mechanism of the yeast pyridoxal 5-phosphate synthase Snz1. *Biochem. J.* **432**, 445-450
- 14 Hanes, J. W., Burns, K. E., Hilmey, D. G., Chatterjee, A., Dorrestein, P. C. and Begley, T. P. (2008) Mechanistic studies on pyridoxal phosphate synthase: the reaction pathway leading to a chromophoric intermediate. *J. Am. Chem. Soc.* **130**, 3043-3052
- 15 Raschle, T., Arigoni, D., Brunisholz, R., Rechsteiner, H., Amrhein, N. and Fitzpatrick, T. B. (2007) Reaction mechanism of pyridoxal 5'-phosphate synthase. Detection of an enzyme-bound chromophoric intermediate. *J. Biol. Chem.* **282**, 6098-6105
- 16 Guédez, G., Hipp, K., Windeisen, V., Derrer, B., Gengenbacher, M., Böttcher, B., Sinning, I., Kappes, B. and Tews, I. (2012) Assembly of the eukaryotic PLP-synthase complex from *Plasmodium* and activation of the Pdx1 enzyme. *Structure.* **20**, 172-184
- 17 Laskowski, R. A. (2001) PDBsum: summaries and analyses of PDB structures. *Nucleic Acids Res.* **29**, 221-222
- 18 Laskowski, R. A. (2009) PDBsum new things. *Nucleic Acids Res.* **37**, D355-D359
- 19 Irwin, J. J. and Shoichet, B. K. (2005) ZINC-a free database of commercially available compounds for virtual screening. *J. Chem. Inf. Model.* **45**, 177-182
- 20 Venkatachalam, C., Jiang, X., Oldfield, T. and Waldman, M. (2003) LigandFit: a novel method for the shape-directed rapid docking of ligands to protein active sites. *J. Mol. Graphics Model.* **21**, 289-307
- 21 Mayo, S. L., Olafson, B. D. and Goddard, W. A. (1990) DREIDING: A generic force field for molecular simulations. *J. Phys. Chem.* **94**, 8897-8909
- 22 Krammer, A., Kirchoff, P. D., Jiang, X., Venkatachalam, C. and Waldman, M. (2005) LigScore: a novel scoring function for predicting binding affinities. *J. Mol. Graphics Model.* **23**, 395-407
- 23 Humphrey, W., Dalke, A. and Schulten, K. (1996) VMD: visual molecular dynamics. *J. Mol. Graphics.* **14**, 33-38
- 24 Müller, I. B., Knöckel, J., Groves, M. R., Jordanova, R., Ealick, S. E., Walter, R. D. and Wrenger, C. (2008) The assembly of the plasmodial PLP synthase complex follows a defined course. *PLoS ONE.* **3**, 1-9
- 25 Knöckel, J., Jordanova, R., Müller, I. B., Wrenger, C. and Groves, M. R. (2009) Mobility of the conserved glycine 155 is required for formation of the active plasmodial dodecamer. *Biochim. Biophys. Acta.* **1790**, 347-350
- 26 Trager, W. and Jensen, J. B. (1976) Human malaria parasites in continuous culture. *Science.* **193**, 673-675
- 27 Das Gupta, R., Krause-Ihle, T., Bergmann, B., Müller, I. B., Khomutov, A. R., Müller, S., Walter, R. D. and Lüersen, K. (2005) 3-Aminoxy-1-aminopropane and derivatives have an antiproliferative effect on cultured *Plasmodium falciparum* by decreasing intracellular polyamine concentrations. *Antimicrob. Agents Chemother.* **49**, 2857-2864
- 28 Lambros, C. and Vanderberg, J. P. (1979) Synchronization of *Plasmodium falciparum* erythrocytic stages in culture. *J. Parasitol.* **3**, 418-420
- 29 Müller, I. B., Wu, F., Bergmann, B., Knöckel, J., Gehring, H., Walter, R. D. and Wrenger, C. (2009) Poisoning pyridoxal 5-phosphate dependent enzymes: a new strategy to target the malaria parasite *Plasmodium falciparum*. *PLoS ONE.* **4**, 1-9
- 30 Derrer, B., Windeisen, V., Guedez Rodriguez, G., Seidler, J., Gengenbacher, M., Lehmann, W. D., Rippe, K., Sinning, I., Tews, I. and Kappes, B. (2010) Defining the structural requirements of ribose 5-phosphate-binding and intersubunit cross-talk of the malarial pyridoxal 5-phosphate synthase. *FEBS Lett.* **584**, 4169-4174

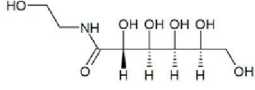
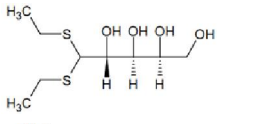
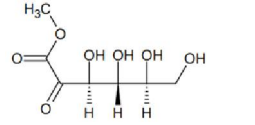
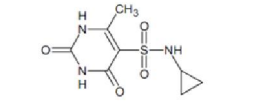
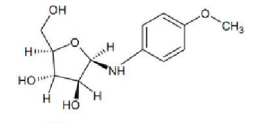
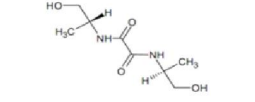
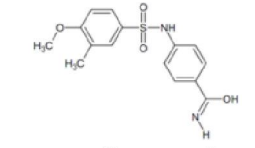
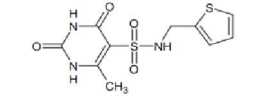
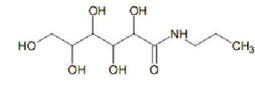
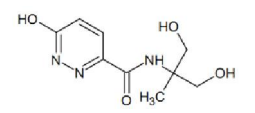
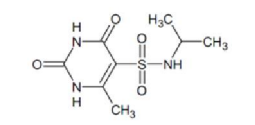
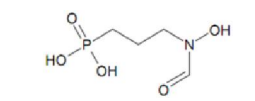
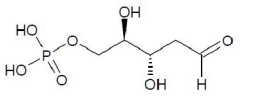
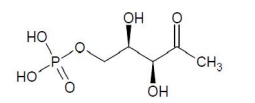
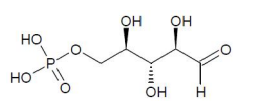
- 31 Zein, F., Zhang, Y., Kang, Y. N., Burns, K., Begley, T. P. and Ealick, S. E. (2006) Structural insights into the mechanism of the PLP synthase holoenzyme from *Thermotoga maritima*. *Biochemistry*. **45**, 14609-14620
- 32 Burgos, E. and Salmon, L. (2004) Synthesis and evaluation of new 4-phospho-D-erythronic acid derivatives as competitive inhibitors of spinach ribose-5-phosphate isomerase. *Tetrahedron Lett.* **45**, 753-756
- 33 Christen, P. and Mehta, P. K. (2001) From cofactor to enzymes. The molecular evolution of pyridoxal-5'-phosphate-dependent enzymes. *Chem. Rec.* **1**, 436-447
- 34 Ehrenshaft, M., Bilski, P., Li, M. Y., Chignell, C. F. and Daub, M. E. (1999) A highly conserved sequence is a novel gene involved in *de novo* vitamin B₆ biosynthesis. *Proc. Natl. Acad. Sci. USA.* **96**, 9374-9378
- 35 Galperin, M. Y. and Koonin, E. V. (1997) Sequence analysis of an exceptionally conserved operon suggests enzymes for a new link between histidine and purine biosynthesis. *Mol. Microbiol.* **24**, 443-445
- 36 Woodruff, W. and Wolfenden, R. (1979) Inhibition of ribose-5-phosphate isomerase by 4-phosphoerythronate. *J. Biol. Chem.* **254**, 5866
- 37 Backhausen, J. E., Jöstingmeyer, P. and Scheibe, R. (1997) Competitive inhibition of spinach leaf phosphoglucose isomerase isoenzymes by erythrose 4-phosphate. *Plant Sci.* **130**, 121-131
- 38 Chirgwin, J., Parsons, T. and Noltmann, E. (1975) Mechanistic implications of the pH independence of inhibition of phosphoglucose isomerase by neutral sugar phosphates. *J. Biol. Chem.* **250**, 7277
- 39 Ruijter, G. J. G. and Visser, J. (1999) Characterization of *Aspergillus niger* phosphoglucose isomerase. Use for quantitative determination of erythrose 4-phosphate. *Biochimie.* **81**, 267-272
- 40 Jeffery, C. J., Bahnson, B. J., Chien, W., Ringe, D. and Petsko, G. A. (2000) Crystal structure of rabbit phosphoglucose isomerase, a glycolytic enzyme that moonlights as neuroleukin, autocrine motility factor, and differentiation mediator. *Biochemistry.* **39**, 955-964
- 41 Burns, K. E., Xiang, Y., Kinsland, C. L., McLafferty, F. W. and Begley, T. P. (2005) Reconstitution and biochemical characterization of a new pyridoxal-5'-phosphate biosynthetic pathway. *J. Am. Chem. Soc.* **127**, 3682-3683
- 42 Fitzpatrick, T. B., Amrhein, N., Kappes, B., Macheroux, P., Tews, I. and Raschle, T. (2007) Two independent routes of *de novo* vitamin B₆ biosynthesis: not that different after all. *Biochem. J.* **407**, 1-13
- 43 Roberts, C. W., Roberts, F., Lyons, R. E., Kirisits, M. J., Mui, E. J., Finnerty, J., Johnson, J. J., Ferguson, D. J. P., Coggins, J. R., Krell, T., Coombs, G. H., Milhous, W. K., Kyle, D. E., Tzipori, S., Barnwell, J., Dame, J. B., Jane, C. and McLeod, R. (2002) The Shikimate Pathway and Its Branches in Apicomplexan Parasites. *J. Infect. Dis.* **185**, S25-S36
- 44 Bozdech, Z. and Ginsburg, H. (2005) Data mining of the transcriptome of *Plasmodium falciparum*: the pentose phosphate pathway and ancillary processes. *Malaria J.* **4**, 17
- 45 Joshi, S., Singh, A. R., Kumar, A., Misra, P. C., Siddiqi, M. I. and Saxena, J. K. (2008) Molecular cloning and characterization of *Plasmodium falciparum* transketolase. *Mol. Biochem. Parasitol.* **160**, 32-41
- 46 Moccand, C., Kaufmann, M. and Fitzpatrick, T. B. (2011) It takes two to tango: defining an essential second active site in pyridoxal 5'-phosphate synthase. *PLoS ONE.* **6**, e16042
- 47 Raschle, T., Speziga, D., Kress, W., Moccand, C., Gehrig, P., Amrhein, N., Weber-Ban, E. and Fitzpatrick, T. B. (2009) Intersubunit cross-talk in pyridoxal 5'-phosphate synthase coordinated by the C terminus of the synthase subunit. *J. Biol. Chem.* **284**, 7706-7718

- 48 Butzloff, S., Groves, M. R., Wrenger, C. and Müller, I. B. (2012) Cytometric quantification of singlet oxygen in the human malaria parasite *Plasmodium falciparum*. *Cytometry A*. **81**, 698-703
- 49 Davis, A. M., Keeling, D. J., Steele, J., Tomkinson, N. P. and Tinker, A. C. Components of Successful Lead Generation. *Curr. Top. Med. Chem.* **5**, 421-439
- 50 Zhao, H. (2007) Scaffold selection and scaffold hopping in lead generation: a medicinal chemistry perspective. *Drug Discov. Today*. **12**, 149-155
- 51 Oyakhrome, S., Issifou, S., Pongratz, P., Barondi, F., Ramharter, M., Kun, J. F., Missinou, M. A., Lell, B. and Kremsner, P. G. (2007) Randomized controlled trial of fosmidomycin-clindamycin versus sulfadoxine-pyrimethamine in the treatment of *Plasmodium falciparum* malaria. *Antimicrob. Agents Chemother.* **51**, 1869-1871
- 52 Borrmann, S., Issifou, S., Esser, G., Adegnika, A. A., Ramharter, M., Matsiegui, P.-B., Oyakhrome, S., Mboumba, D. P. M., Missinou, M. A., Kun, J. F. J., Jomaa, H. and Kremsner, P. G. (2004) Fosmidomycin-clindamycin for the treatment of *Plasmodium falciparum* malaria. *J. Infect. Dis.* **190**, 1534-1540

Tables and Figures

Table 1: *In silico*-identified compounds tested against PfPdx1. Several pharmacophores generated for PfPdx1 were screened to obtain best-fitting ligands which were, together with rationally selected compounds, subjected to additional docking into PfPdx1 homology models. R5P was used as a control during docking simulations. Resultant compounds were tested on purified PfPdx1 (see the Experimental section). Values in parentheses indicate scores calculated for ligands docked into PbPdx1. Values are from three or more independent experiments performed in duplicate, with the standard error of the mean (SEM) indicated.

Compound	Structure	LigScore 1 ^a	LigScore 2 ^a	Dock score ^b	Conc. (mM)	PfPdx1 inhibition (% residual activity)
1		6.17	5.6	44.91	0.5	96 ± 3
2		5.75	5.39	61.35	0.5	103 ± 4
3		5.97	5.51	54.76	3	96 ± 5
4		5.22	4.94	82.18	3	96 ± 3
5		4.76	5.36	24.01	0.5	99 ± 5

6		6.14	5.71	40.09	0.5	107 ± 6
7		5.4	6.03	33.31	1	99 ± 7
8		6.21	5.87	45.38	0.5	88 ± 6
9		4.55	4.95	44.91	1	113 ± 2
10		6.87	6.24	49.51	0.5	200 ± 20 *
11		4.97	4.93	32.52	0.5	110 ± 10
12		5.6	5.9	34.71	0.5	107 ± 5
13		5.27	6.02	42.14	0.5	99 ± 3
14		5.65	5.05	41.51	0.5	99 ± 5
15		4.85	5.79	42.94	0.5	95 ± 4
16		4.5	5.28	41.49	0.5	105 ± 3
17		6.27	5.99	91.33	20	103 ± 8
18		6.69	6.47	85.64	12	56 ± 4 ** (Fig 1A)
19		6.64	6.29	88.92	5	88 ± 4
R5P		6.55 (4.32)	6.02 (2.63)	90.15 (107.14)	-	Substrate (control)

G3P		5.87	5.36	82.83	-	Substrate
PLP		6.51	6.27	90.36	-	Product

Footnotes: ^aLigScore1 and LigScore2, with units of pKi (-log Ki), refers to predicted receptor-ligand binding affinities. ^bDockscore refers to the unitless rigid body minimization energy of the final ligand pose calculated during Monte Carlo trials. * absorbance of compound interfered with detection of PLP. ** $P < 0.10$ in a two-sided t-test.

Table 2: E4P analogues and their efficacy on PfPdx1. Selected compounds were docked into a PfPdx1 homology model and poses were evaluated using LigScore ligand pose scoring functions. R5P was used as a control during docking simulations, with Ligscore and Dockscore values listed in Table 1. Values in parentheses indicate scores calculated for ligands in Pbpdx1. IC₅₀ values were calculated from dose-response curves of the respective compounds incubated with purified PfPdx1, as reported in the Experimental section. IC₅₀ values represent data from three or more independent experiments performed in duplicate, with the SEM indicated.

Compound	Structure	LigScore1 _a	LigScore2 _a	Dock score _b	IC ₅₀ on PfPdx1
E4P		6.40 (3.00)	6.09 (0.41)	85.17 (120.89)	3.7 ± 0.9 mM
D-erythrose		4.74	4.25	42.19	160 ± 46 mM
EHZ		5.34	5.39	53.48	902 ± 206 μM
4PEHZ		6.55 (3.73)	6.43 (1.46)	98.96 (117.01)	43 ± 8 μM

Footnotes: ^aLigScore1 and LigScore2, with units of pKi (-log Ki), refers to predicted receptor-ligand binding affinities. ^bDockscore refers to the unitless rigid body minimization energy of the final ligand pose calculated during Monte Carlo trials.

Figure 1. Effect of alternative sugar substrates on *PfPdx1*. (A) Inhibition of *PfPdx1* by DR5P. Representative UV-visible absorbance spectra of *PfPdx1* incubated with increasing concentrations of DR5P. Decreased levels of PLP, visible as diminished 414 nm PLP-Schiff base absorbance, correlated with increased concentrations of DR5P. (B) potential utilisation of alternative sugars by *PfPdx1*. Representative UV-visible absorbance spectra of *PfPdx1* incubated with 3 mM R5P or E4P, and 12 mM F6P or DR5P in the presence of G3P. Only R5P supported formation of PLP visible at 414 nm, and in the absence of G3P (- G3P) the I₃₂₀ specie could be formed from R5P. A 320 nm maximum absorbance peak was observed for E4P. (C) R5P docked into *PbPdx1* using LigandFit. The ligand poses or receptor-ligand binding affinities were calculated using LigScore1, with units of pK_i (-log K_i), in which R5P could be docked back into the structure with a score of 4.32. (D) E4P docked into the R5P binding site of *PbPdx1*. The molecule was predicted to hydrogen bond with K84, mainly involving the aldehyde and hydroxyl groups, similarly interacting with residue D27. E4P was calculated to have a LigScore1 of 3.00.

Figure 2. Inhibitory effect of E4P on *PfPdx1*. (A) Representative UV-visible absorbance spectra of *PfPdx1* incubated with increasing concentrations of E4P, which affected both PLP production and the formation of I₃₂₀. (B) IC₅₀ of E4P and D-erythrose. The IC₅₀ of E4P was calculated as 3.7 ± 0.9 mM and D-erythrose as 160 ± 46 mM. Values represent data from three independent experiments performed in duplicate compared to an uninhibited control, error bars represent the standard error of the mean (SEM) given with the 95% confidence interval in dotted lines.

Figure 3. Formation of R5P-related I₃₂₀ with *PfPdx1* variants. (A) Wild-type (WT), DKK (D26A, K83A and K151A) and ERR (E136A, R139A and R140A) variants of *PfPdx1* were incubated with 0.5 mM R5P and 20 mM NH₄Cl. 100 µg of each Pdx1 variant was present, except for the DKK mutant represented with 19.8 µg protein. Positive control reactions WT (R5P and G3P) included 0.5 mM G3P to demonstrate active protein, with PLP formation visible at 414 nm. I₃₂₀ formation was evident in WT (R5P) protein which was solely incubated with R5P. The ERR *PfPdx1* (R5P) mutant showed formation of I₃₂₀, whereas the DKK mutant did not form this species underscoring the importance of the DKK residues. (B) WT, ΔC and RHE (R85A, H88A and E91A) *PfPdx1* variants were incubated with R5P. 100 µg of each protein variant was used in the assay. In both ΔC and RHE I₃₂₀ formation was abolished. (C) Activity of WT and R167A *PfPdx1*. The assay contained 100 µg of each protein. The R167A *PfPdx1* protein had reduced PLP-producing capability and in the presence of only R5P the formation of I₃₂₀ was diminished compared to WT *PfPdx1*.

Figure 4. E4P analogues and their effect on *PfPdx1*. (A) 4PEHz docked into *PbPdx1*. Poses of 4PEHz were scored using LigScore1 and resulted in a value of 3.73, compared to 4.32 for the R5P control substrate. The hydrazide group of 4PEHz was oriented approximately parallel to R150 in close proximity to D108, where both ketone and the hydroxyl substituents of 4PEHz hydrogen bonded with K84 and D27. (B) Representative UV-visible absorbance spectra of *PfPdx1* with increasing concentrations of 4PEHz which resulted in decreased formation of PLP visible at 414 nm. Formation of a 320 nm absorbing species was observed similar to E4P. Results represent single observations from independent triplicate experiments. (C) Efficacy of 4PEHz and EHz on purified *PfPdx1* with 4PEHz calculated to have an IC₅₀ of 43 ± 8 µM and EHz an IC₅₀ of 0.9 ± 0.2 mM. (D) Effect of 4PEHz on the *PfPdx1* activity contained in the PLP synthase. Reaction conditions included 20 mM glutamine, 0.5 mM R5P

and G3P, with 100 μg of both *PfPdx1* and *PfPdx2*. 4PEHz had an IC_{50} of $16 \pm 4 \mu\text{M}$. Values in C and D represent data from three independent experiments performed in duplicate compared to an uninhibited control, in which error bars indicate the SEM, together with the 95% confidence interval in dotted lines.

Figure 5. Efficacy of 4PEHz on the proliferation of intra-erythrocytic *P. falciparum* parasites. (A) Parasite proliferation was assessed by monitoring the [^3H]-hypoxanthine incorporation. After 48 h parasite proliferation was reported as the percentage of [^3H]-hypoxanthine incorporation compared to that for uninhibited control parasites. The IC_{50} for 4PEHz was $10.4 \pm 1.2 \mu\text{M}$, compared to $138 \pm 9 \mu\text{M}$ for EHz. Values represent data from more than three independent experiments performed in triplicate, where error bars represent the SEM together with the 95% confidence interval in dotted lines. (B) The growth of *PfPdx1/PfPdx2*-complemented and mock-control parasites was determined in the presence of 1 μM 4PEHz. The parasitemia (% infected erythrocytes per 1000 erythrocytes) of the treated parasites was compared to untreated parasites and expressed as a percentage growth relative to the untreated control. Results represent average values from two independent experiments performed in triplicate, of which error bars indicate the SEM. Comparisons between treated and untreated parasites were made using an unpaired two-tailed Student's t-test in which ** represents statistical significance ($p < 0.05$). The mock parasites were significantly affected after 48 h, and had diminished growth over the 168 h period. Parasites complemented with *PfPdx1* and *PfPdx2* were not significantly affected by 4PEHz treatment, suggesting that 4PEHz affects PLP-related processes within the parasites, and complementation of PLP biosynthesis protects these parasites from the *PfPdx1* inhibitor.

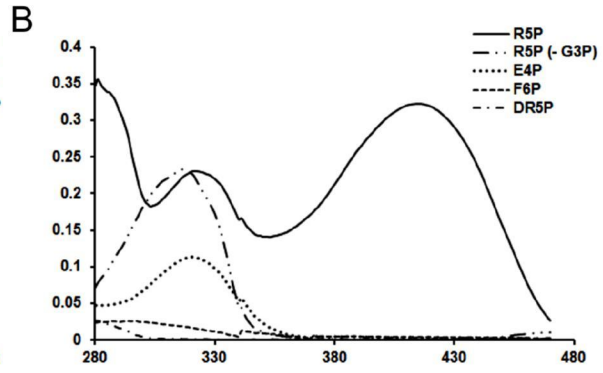
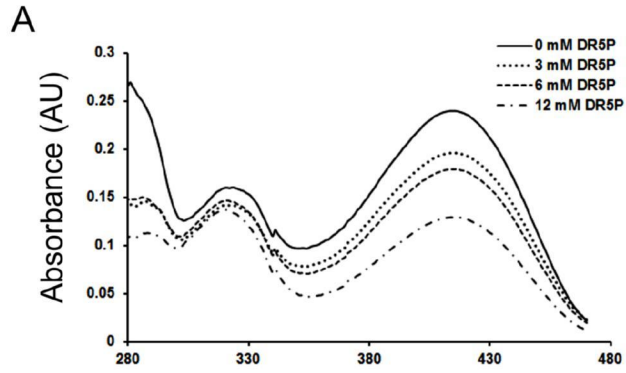
Figure 6. Schematic illustration of the formation of PLP from R5P, G3P and L-glutamine, as adapted from Hanes *et al* [10]. Initial binding of R5P in Pdx1 entails imine formation of the C1 of R5P with K83. Following binding, R5P undergoes isomerization, imine formation with ammonia, as well as a C1 to C5 lysine migration. Loss of phosphate results in the formation of I_{320} , followed by imine formation with G3P, which leads to ring closure and formation of PLP. E4P and 4PEHz both inhibit *PfPdx1* and share polyhydroxyl stereochemical arrangement and contain hydrolyzable phosphate groups similar to R5P. E4P contains a C1 aldehyde group, which is proposed to functionally mimic similar groups in R5P, and could facilitate entry into the *PfPdx1* R5P-active site. 4PEHz, with a terminal hydrazide group, may similarly enter the active site, and interfere with PLP formation.

Supplementary Figure 1: Detection of PLP is not affected by E4P. Standard curves of PLP, containing concentrations ranging from 10 μ M to 200 μ M PLP with no E4P (A), or containing 1 mM (50 nmol) E4P (B), in Tris-HCl buffer conditions including 0.5 mM R5P and G3P with 20 mM NH_2Cl . Reactions were incubated at 37 $^\circ\text{C}$ for 1.5 h. Statistical analyses of the linear regression slope and intercepts revealed no significant differences in the slopes of the two different regression lines ($P = 0.975$). Similarly, ANCOVA showed no significant difference ($P = 0.401$) between the two regression lines. Results represent data from four independent experiments performed in triplicate. This verifies that molar excess concentrations of E4P did not affect detection of the PLP-Schiff base formed at 414 nm.

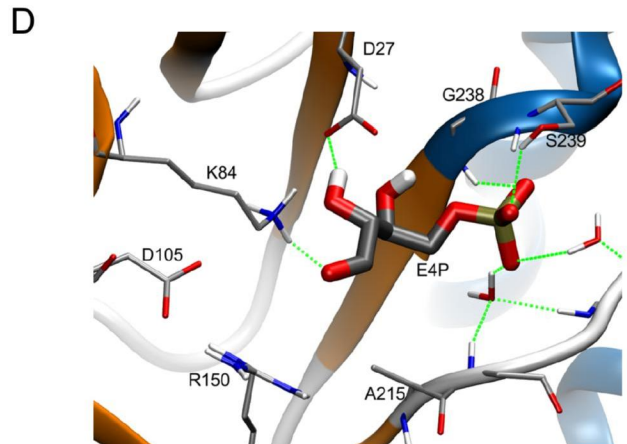
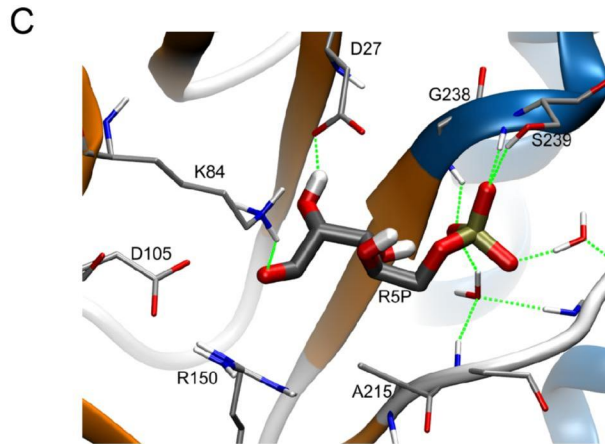
Supplementary Figure 2: Effect of 4PEHz on mock and *PfPdx1/PfPdx2* over-expressing transgenic parasites. Mock control cells (A) and *PfPdx1/PfPdx2* over-expressing cells (B) were treated with 1 μ M 4PEHz in continuous culture for seven days. The cumulative parasitemia was calculated from the observed parasitemia taking the dilution factor into account. The data represents average values from two independent experiments performed in triplicate, in which error bars indicate the SEM. Statistical analyses using GraphPad Prism tested a null hypothesis that the lines were the same with a 99% confidence interval ($P = 0.01$, $F = 0.01$). Mock-UT and Mock-T (B) had significantly different slopes ($P < 0.0001$). Whereas *PfPdx1/PfPdx2*-UT and *PfPdx1/PfPdx2*-T (C) did not have significantly different slopes ($P = 0.0138$). Similarly ANCOVA analyses comparing MOCK-UT with MOCK-T revealed that the lines differed significantly (F-ratio probability < 0.0001), whereas *Pdx1/2*-UT did not significantly differ from *PfPdx1/PfPdx2*-T (F-ratio probability = 0.0986).

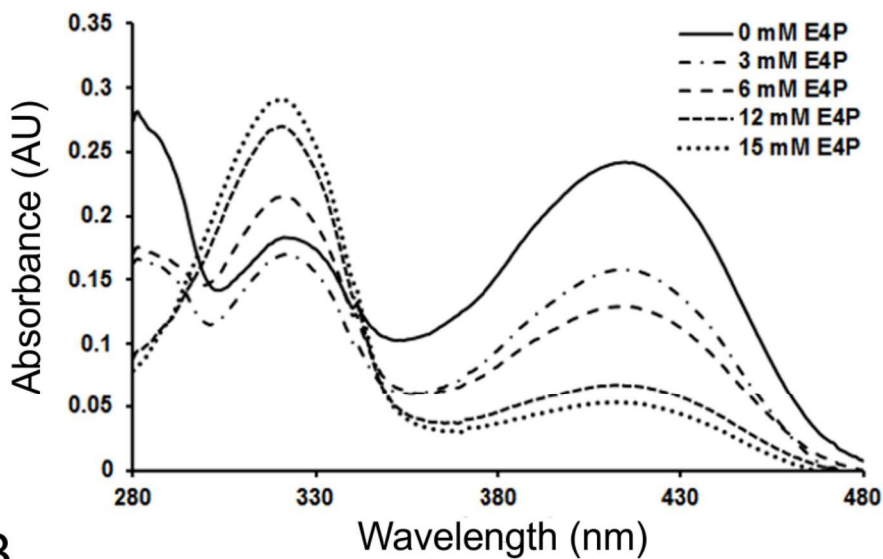
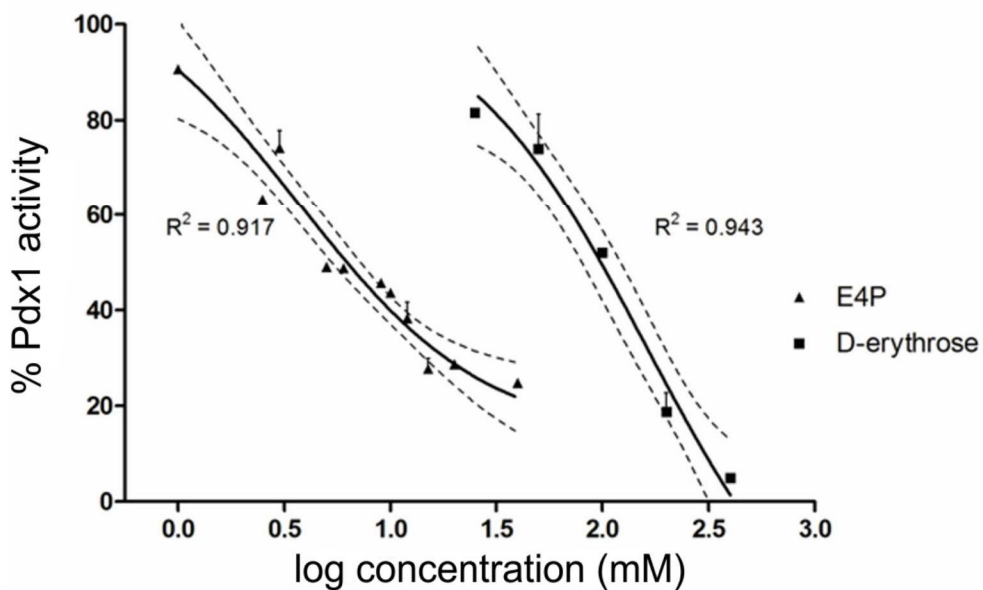
Supplementary figure 3: Composition of parasite stages in mock control parasites during long-term exposure of 4PEHz. The parasite life-stage composition (percentage of rings, trophozoites or schizonts) of untreated (A) and treated (B) *P. falciparum* mock cells was determined microscopically during long term growth assays. Results represent average values from two independent experiments performed in triplicate, of which error bars indicate the SEM. Comparisons between treated and untreated mock parasites were made using an unpaired two-tailed Student's t-test in which ** represents statistical significance ($p < 0.05$). The treated mock parasites had a significantly different ring and trophozoite life-stage composition compared to the untreated controls parasites at 120 hours while all other time points did not reveal significant differences in the life-stage compositions.

Supplementary figure 4: Composition of parasite stages in *PfPdx1/PfPdx2*-complemented parasites during long-term exposure of 4PEHz. The parasite life-stage composition (percentage of rings, trophozoites or schizonts) of untreated (A) and treated (B) *P. falciparum PfPdx1/PfPdx2*-overexpressing parasites was determined microscopically during long term growth assays. Results represent average values from two independent experiments performed in triplicate, of which error bars indicate the SEM. Comparisons between treated and untreated mock parasites were made using an unpaired two-tailed Student's t-test in which ** represents statistical significance ($p < 0.05$). There were no significant differences in the life-stage compositions between untreated and treated *PfPdx1/PfPdx2* parasites at any of the time points. This confirmed that complementation of PLP biosynthesis protected the parasites from the effects of 4PEHz, and the parasites grew normally compared to untreated cells.

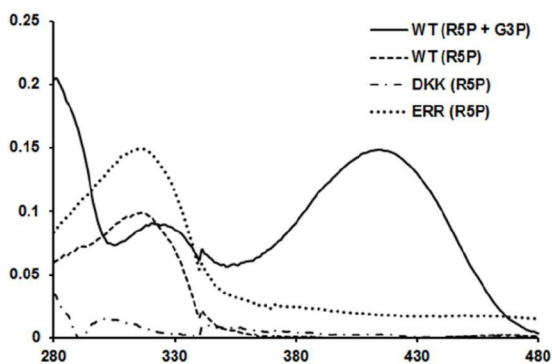


Wavelength (nm)

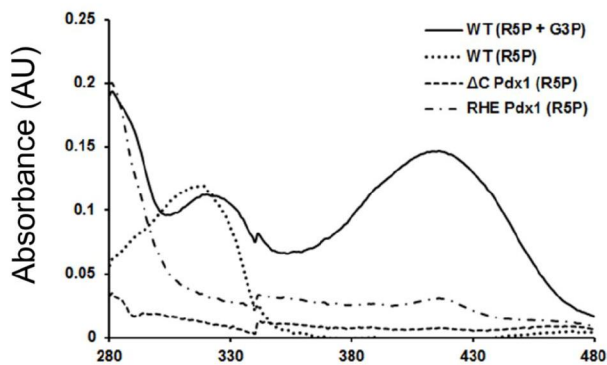


A**B**

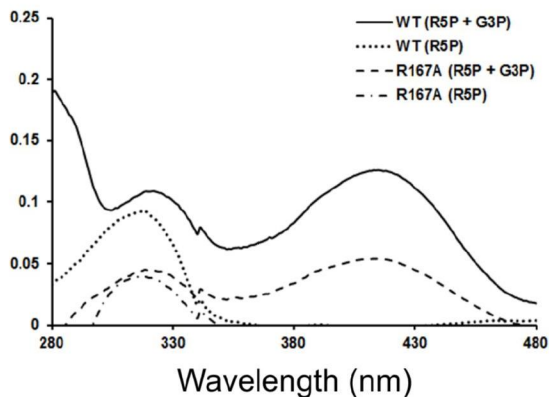
A

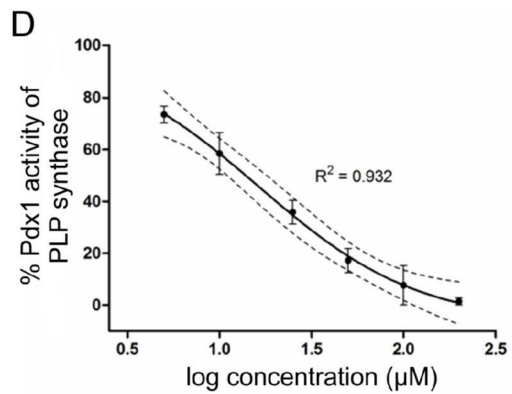
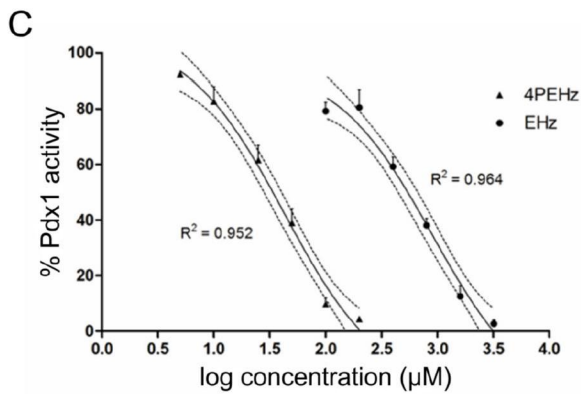
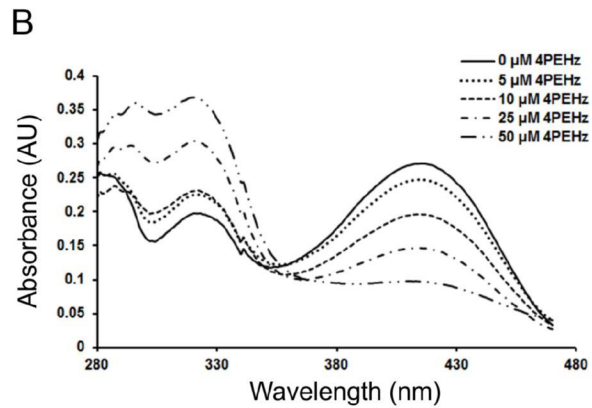
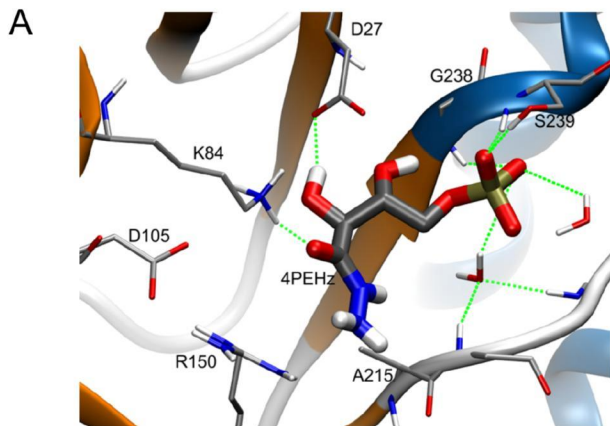


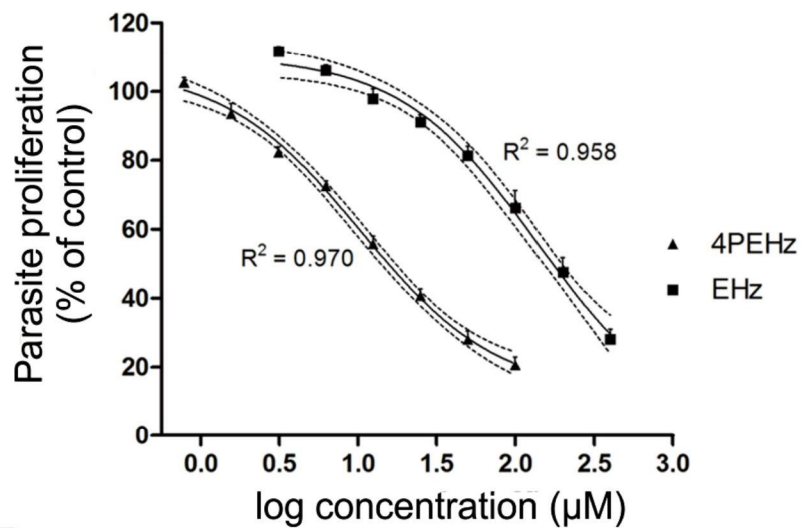
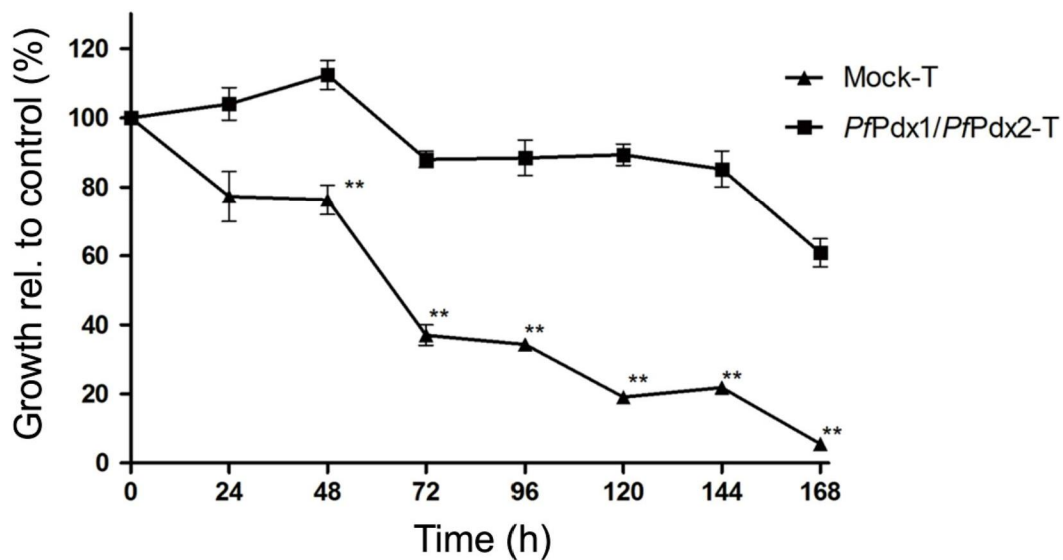
B

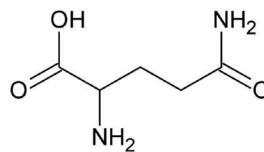
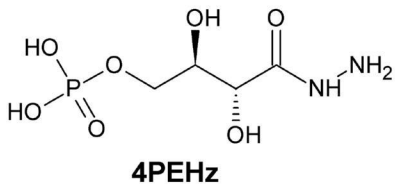
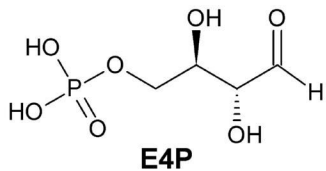


C



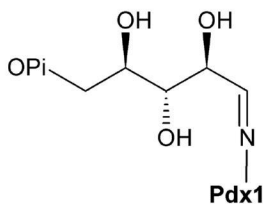
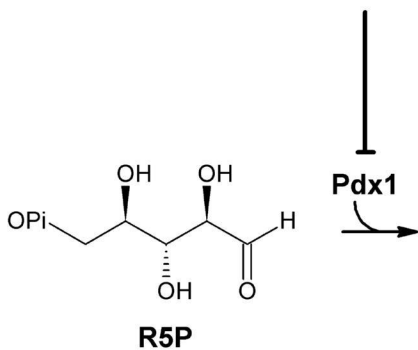


A**B**

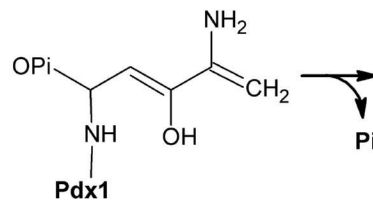


L-glutamine

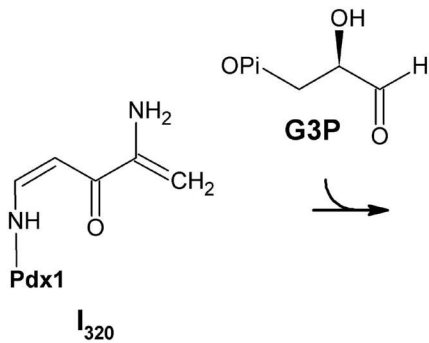
↓ **Pdx2**



NH₃



↓ **Pi**



I₃₂₀

